Non-Additive Cost Functions for Color Image Steganography Based on Inter-Channel Correlations and Differences

Yaofei Wang, Weiming Zhang, Weixiang Li, Xinzhi Yu, and Nenghai Yu

***Abstract*— Despite the strong presence of color images for communication, scholars have mainly devoted their attention to research on steganography for grayscale images. In contrast to grayscale images, color images have three interrelated color channels, and the relationships among the three channels have a strong impact on the steganography security. In this paper, we present a steganographic scheme for spatial color images by exploiting the correlations and differences between the color channels. We find that the G channel has a stronger correlation with R and B than the one between R and B, and thus, synchronizing the modification directions of the R and B channels with those from the G channel will have better resistance to detection. In addition, the payload capacity and the distribution of complex regions between channels are different. Based on these findings, we design a new strategy for defining non-additive costs for color image steganography, called G-channel-related Inter-channel Non-Additive (GINA) strategy. The GINA strategy can make the modification directions of the R and B channels consistent with those of the G channel and can adaptively distribute the embedding capacity between the three channels. Specifically, this strategy will not violate the Complexity Prior rule. The experimental results show that the proposed GINA strategy can significantly improve the performance in terms of resisting color image steganalysis compared with previous methods.**

***Index Terms*— Color image steganography, steganalysis, inter-channel correlation, non-additive cost.**

I. Introduction

STEGANOGRAPHY is the art and science of hiding information in objects to keep information confidential and prevent the detection of hidden messages [1], [2]. In recent years, the most successful scheme is content-adaptive steganography based on the minimum distortion embedding framework, which tends to embed secret messages into textured and noisy regions, making them difficult to detect by steganalysis. The distortion is obtained by assigning a cost to each cover element. A distortion function is considered additive when it is expressed as a sum of costs, which element-wisely evaluate the effect of respective embedding modification.

Since the Syndrome-Trellis Code (STC) [3] performs well in minimizing the additive distortion, general steganographic schemes mainly focus on the design of the additive cost function. Various popular additive cost functions, such as HUGO (highly undetectable stego) [4], WOW (wavelet obtained weights) [5], S-UNIWARD (spatial-universal wavelet relative distortion) [6], HILL (high-pass, low-pass, and low-pass) [7], MG (Multivariate Gaussian), and MiPOD (Minimizing the Power of Optimal Detector) [8] exist for grayscale image steganography.

Intuitively, the non-additive distortion model is more suitable for natural images because the changes on adjacent pixels will interact. The first important rule in how to exploit the mutual impact of adjacent modifications was proposed by Li *et al.* [9] and Denemark and Fridrich [10] independently. This rule is called Synchronizing Modification Directions (SMD) or Clustering Modification Directions (CMD). The rule implies that synchronizing the modification directions of adjacent pixels can significantly improve the anti-detection performance. In [9] and [10], the ± 1 modifications are used for embedding messages, and the adjacent pixels are separated into sub-images. The initial costs are obtained with an additive cost function and then updated according to the directions of the modified adjacent pixels in the other embedded sub-images. We call the strategy used in [9] and [10] the "Updating Cost" (abbreviated to UpCost) method. Because designing efficient coding scheme for non-additive cost functions is an important open problem in steganography [11], Zhang *et al.* [12] proposed a novel framework called DeJoin by defining a joint distortion on pixel blocks and then decomposing this distortion into additive distortion on individual pixels. It has been proven that DeJoin can approach the lower bound of average joint distortion for a given payload.

In recent research on steganography, grayscale images have received substantial attention as mentioned above. Most studies have focused on grayscale images with the unspoken assumption that the findings can be applied directly to color images. However, this view ignores the crucial fact that there is a strong correlation between the color channels that should be of interest in color image steganography. As early as 2013, some important open problems for moving steganography and steganalysis into the real world were proposed, and the authors called for more attention to the color images [11].

Manuscript received May 3, 2019; revised September 8, 2019 and November 11, 2019; accepted November 21, 2019. Date of publication November 28, 2019; date of current version January 30, 2020. This work was supported in part by the Natural Science Foundation of China under Grant U1636201 and Grant 61572452 and in part by the Anhui Initiative in Quantum Information Technologies under Grant AHY150400. The associate editor coordinating the review of this manuscript and approving it for publication was Dr. Patrick Bas. *(Corresponding author: Weiming Zhang.)*

The authors are with the CAS Key Laboratory of Electro-Magnetic Space Information, University of Science and Technology of China, Hefei 230026, China (e-mail: zhangwm@ustc.edu.cn).

Digital Object Identifier 10.1109/TIFS.2019.2956590

Image communication between people on social networks is generally with color images and several rich models for color image steganalysis have been proposed [13]–[21]; nevertheless, there has been minimal work on color image steganography. To develop color image steganography, we can learn and use the knowledge of grayscale images steganography. There are two directions on extending grayscale images content-adaptive steganography.

The first direction is to design a suitable additive cost function for color images considering the inter-channel correlations. To the best of our knowledge, the only additive cost function for color images was proposed in [22] by Liao et al. The authors exploited inter-channel correlations to allocate payload for the three channels and proposed a novel channel-dependent payload partition strategy based on amplifying channel modification probabilities (ACMP). The ACMP strategy could cluster the embedding impacts of RGB channels and make the modifications concentrate in textured regions, thereby achieving better statistical undetectability against the color rich-model steganalytic feature.

The second direction is to define the non-additive cost functions for color images. In grayscale image steganography, SMD is a very effective rule. The natural idea is to extend SMD to color images. Inspired by the outstanding performance of the CMD strategy, Tang et al. proposed a strategy to cluster modification directions for color images by using the method of UpCost, named CMD-C [23]. This method can synchronize the directions of modifications between different channels in the same location and maintain the color channel correlations. In [24], Qin et al. proposed another steganographic scheme for color images by considering color pixel vectors (CPVs), where three color components from the same pixel location form a vector. The embedding costs are defined directly on the color pixel vectors rather than on a single color component, therefore, the correlations between channels can be explicitly considered. With the help of DeJoin, the vector-based costs can be transformed into component-based costs.

Although CMD-C and CPVs have considered the correlations between color channels, they did not discover the differences in these correlations. In this paper, we further exploit the inter-channel correlations and the differences between channels. Our findings are as follows. First, the G channel has a stronger correlation with the R and B channels than that between the R and B channels, and thus, synchronizing the modification directions of the R and B channels with those from the G channel will achieve greater resistance to detection. Second, the G channel is usually a smooth channel that should have a lower payload capacity, and synchronizations with the G channel will have a relatively low change rate (defined as the ratio of the modified pixels over the total number of pixels). Third, although the contents of the three channels are similar, the distribution of complex regions is different. When updating the costs according to the modifications of the G channel, it should under the Complexity Prior rule. Based on these findings, we extend the SMD rule of grayscale images to Intra-channel-SMD and Inter-channel-SMD rules for color images and design a new strategy based on the two rules for defining a non-additive cost for color image steganography, called G-channel-related Inter-channel Non-Additive (GINA). We present a novel steganographic algorithm that updates the costs according to the GINA. Specifically, we decompose a color image into three channel images, and then, each channel is decomposed into several non-overlapping sub-images. The costs of the pixels are first initialized by an additive cost function. The G channel image is embedded first using the CMD strategy. Then, the costs in the sub-images of the R and B channels are updated according to the modification directions of the same position of the G channel and the adjacent pixels in the same channel. Because the costs are dynamically updated, non-additivity is implicitly introduced into the overall distortion. Considering the different payload capacity of each channel, we adopt the simple color concatenation (SCC) strategy to automatically distribute the payload across color channels. Considering that the distribution of complex regions between three channels varies, we propose a method to select the complex regions to update the costs in the R and B channels according to the modifications of the G channel, which can satisfy the Complexity Prior rule. The proposed GINA strategy can be combined with state-of-the-art steganographic schemes, such as HILL and S-UNIWARD. The experimental results show that the proposed non-additive steganographic strategy can achieve better undetectability than CMD [9], CMD-C [23], CPVs [24] and ACMP [22] against the color image steganalysis.

The main contributions of this paper are summarized as follows:

1) We extend the SMD rule for grayscale images to the Intra-channel-SMD rule and Inter-channel-SMD rule for color images. The Inter-channel-SMD rule is only applied to strongly correlated channels on the premise that the Complexity Prior rule is satisfied.
2) In RGB color images, we found that the G channel has a higher correlation with the other two channels and a lower payload capacity. Based on these findings, we proposed a novel strategy called GINA for color image steganography. To the best of our knowledge, this is the first non-additive strategy for color images that considers both the correlations and the differences between channels.
3) We compared the GINA-based method with different color images steganographic methods and conducted extensive experiments on image datasets with different demosaicking, colorspace and resizing methods. The experimental results proved the superiority of the GINA strategy.

The rest of this paper is organized as follows. In Section II, we briefly introduce the model of minimizing additive distortion and then review the previous rules in grayscale image steganography. In Section III, we first explore the correlations between channels and extend the SMD rule, and then propose the GINA strategy. In Section IV, we show the differences in the payload capacity and distribution of complex regions between channels and then propose a method to select complex regions to apply the Inter-channel-SMD rule. We give an embedding algorithm that can implement the GINA strategy in Section V. In Section VI, the experimental results are given and analyzed. Finally, we conclude the paper in Section VII.

II. Preliminaries

A. Notations

Throughout the paper, matrices, vectors and sets are written in bold face. The color images are in the RGB (red, green, blue) color space and every pixel has three color components. For simplicity, the three channels are denoted as **R**, **G** and **B**. The cover image (of size $n_1 \times n_2 \times 3$) is denoted by $\mathbf{X} = (x_{i,j,k})^{n_1 \times n_2 \times 3}$, $x_{i,j,k} \in \{0, 1, \cdots, 255\}$, $1 \le i \le n_1$, $1 \le j \le n_2$, $k \in \{1, 2, 3\}$. We use the numbers 1, 2 and 3 to represent the three channels **R**, **G** and **B**, respectively. $\mathbf{Y} = (y_{i,j,k})^{n_1 \times n_2 \times 3}$ denotes the stego image. The embedding operation on $x_{i,j,k}$ is formulated by the range I. An embedding operation is called binary if $|I| = 2$ and ternary if $|I| = 3$ for all i, j, k. In this paper, we only discuss the ternary embedding, in which one pixel has two directions of modifications. Therefore, one pixel has three costs: $\rho^{+}_{i,j,k}$, $\rho^{-}_{i,j,k}$ and $\rho^{0}_{i,j,k}$. The $\rho^{+}_{i,j,k}$ means the cost of increasing the pixel by one, and the $\rho^{-}_{i,j,k}$ means the cost of decreasing the pixel by one. The $\rho^{0}_{i,j,k}$ is the cost of not changing, and we assume its value is 0.

B. Minimal Distortion Steganography

In the model established in [3], the cost of modifying a color component pixel value $x_{i,j,k}$ to $y_{i,j,k}$ can be simply denoted by $\rho(y_{i,j,k})$. Denote $\pi(y_{i,j,k})$ as the probability of changing $x_{i,j,k}$ to $y_{i,j,k}$. The sender can send up to $H(\pi)$ bits of message and with total distortion D_π such that

$$H(\pi) = \sum_k H\left(\pi_{\lambda_k}\right), D_\pi = \sum_k D_{\pi_{\lambda_k}} \tag{1}$$

where

$$H\left(\pi_{\lambda_k}\right) = -\sum_i \sum_j \sum_{t_{i,j,k} \in I_{i,j,k}} \pi_{\lambda_k}\left(t_{i,j,k}\right) \log\left(\pi_{\lambda_k}\left(t_{i,j,k}\right)\right) \tag{2}$$

$$D_{\pi_{\lambda_k}} = \sum_i \sum_j \sum_{t_{i,j,k} \in I_{i,j,k}} \pi_{\lambda_k}(t_{i,j,k}) \rho(t_{i,j,k}) \tag{3}$$

For a given message length L, the sender wants to minimize the total distortion D_π. However, different schemes will produce different results. In the traditional framework, the embedding payload is evenly distributed across each color channel; we call this the Average strategy, which can be formulated as the following optimization problem:

$$D^{Average}_{\pi} = min\left(D_{\pi_{\lambda_1}}\right) + min\left(D_{\pi_{\lambda_2}}\right) + min\left(D_{\pi_{\lambda_3}}\right) \tag{4}$$

$$\text{s.t. } H\left(\pi_{\lambda_k}\right) = L/3. \tag{5}$$

Conversely, when we use the SCC strategy, the three channels are concatenated into one to produce a monochromatic image. Thus, we can adaptively distribute the messages across the monochrome image, and the optimization problem becomes

$$D^{SCC}_{\pi} = min\left(\sum_k D_{\pi_{\lambda_k}}\right), \tag{6}$$

$$\text{s.t. } H(\pi) = L. \tag{7}$$

The optimal π follows a Gibbs distribution:

$$\pi_{\lambda_k}(y_{i,j,k}) = \frac{exp(-\lambda_k \rho(y_{i,j,k}))}{\sum\limits_{t_{i,j,k} \in I_{i,j,k}} exp(-\lambda_k \rho(t_{i,j,k}))}, \tag{8}$$

The scalar parameter $\lambda_k > 0$ is determined by payload constraint (5) or (7). In the SCC strategy, we can obtain the suitable payloads C_1, C_2 and C_3 that each channel can embed:

$$C_k = -\sum_i \sum_j \sum_{t_{i,j,k} \in I_{i,j,k}} \pi_{\lambda_k}\left(t_{i,j,k}\right) \log\left(\pi_{\lambda_k}\left(t_{i,j,k}\right)\right) \tag{9}$$

In this paper, we will first calculate the suitable payload for each channel using the SCC strategy, according to that the messages of corresponding payloads are assigned to three channels. In the same channel, we evenly divide the messages into sub-images, as done in traditional methods [9] [23].

C. Four Rules in Cost Assignment

In previous steganographic schemes, four rules for designing cost functions have been proposed for grayscale images. These rules for cost assignment can be summarized as follows:

1) *Complexity Prior:* The most important rule is the Complexity Prior. Its philosophy is to assign lower costs to the pixels in the textured and noisy regions. Because the non-periodical textured and noisy regions are difficult to model, making modifications in such regions often leads to slight deviations in the steganalytic feature space, and thus is more difficult to detect. Many methods proposed in [4]–[7] follow this rule explicitly.
2) *Spreading:* The second rule is called the Spreading rule [25], which requires that the costs of two neighboring pixels not differ significantly. In other words, a pixel with high or low priority should spread its high rank or low rank to its neighbours. In this way, a pixel close to a complex region will have higher priority than a pixel close to the smooth region even though these two pixels have the same cost after using the cost function. The Spreading rule has been successfully utilized in the spatial domain [25] and DCT domain [26].
3) *Controversial Pixels Prior:* The third rule is called the Controversial Pixels Prior (CPP) rule [27], which was proposed by Zhou et al. The CPP rule considers a combination of several methods that have comparable security performance and gives priority for modification to the pixels with very distinguishing costs calculated by different cost functions.
4) *Synchronizing Modification Directions:* The above three rules are based on the additive distortion model, in which the changes of pixels are assumed to be independent. However, the changes of neighboring pixels will interact with each other, and thus, it will be more suitable for adaptive steganography with a non-additive distortion model. The first important rule based on the non-additive distortion was proposed by Li *et al.* [9] and Denemark and Fridrich [10] independently. This rule is called Synchronizing Modification Directions (SMD) or Clustering Modification Directions (CMD). This rule aims at synchronizing the modification directions of adjacent pixels.

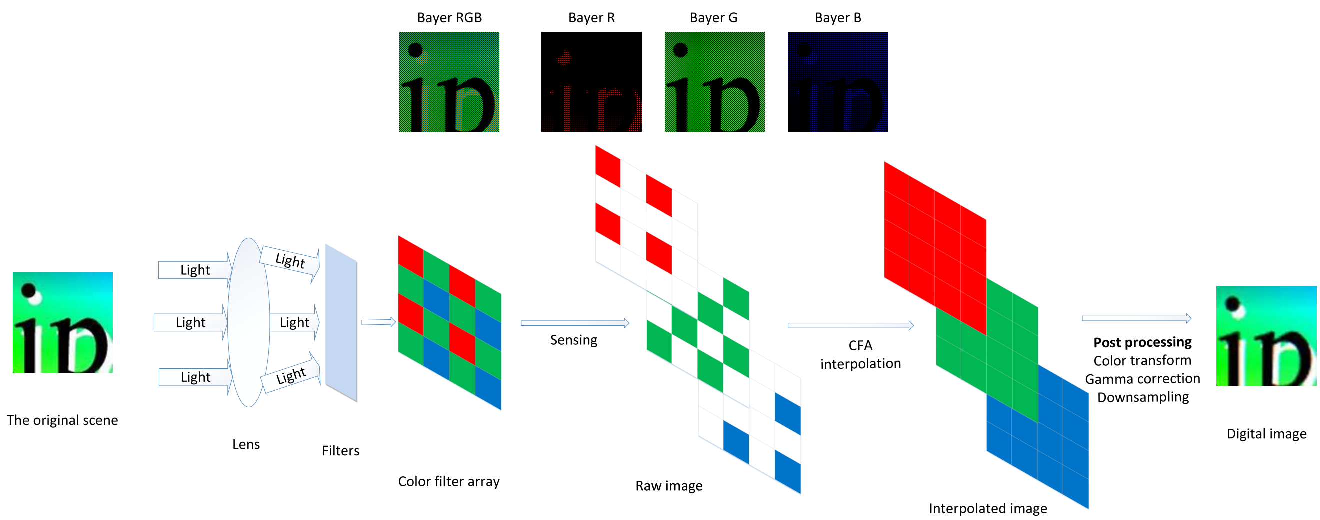

Fig. 1. Image capture process in a digital camera.

Soon after, Zhang *et al.* [12] proposed a novel framework called DeJoin for minimizing non-additive distortion in steganography.

III. G-Channel-Related Inter-Channel Non-Additive Strategy

In the previous section, four rules for grayscale images for assigning cost functions are revisited. Because the method of obtaining the initial cost in the color images is the same as that for grayscale images, we assume that those rules that are based on the additive distortion model can also be used in the color images. However, for the SMD rule, we assume that it needs to be modified for the color images when considering the correlations between channels. In this section, we will extend the SMD rule and propose a new strategy for color images. We validate the effectiveness of this strategy in a series of simulations. The simulations are performed on a color version of BOSSbase 1.01 [28] containing 10,000 color $512 \times 512 \times 3$ images. We call this dataset BOSSbasePPGBIC, which is obtained as follows. We first use dcraw (ver. 9.26) for demosaicking full-resolution raw images and then down-sampling the obtained images such that the smaller image dimension is 512 and for central cropping to 512×512. The demosaicking algorithm used in dcraw is the Patterned Pixel Grouping (PPG). By default, dcraw writes PPM with 8-bit samples, a BT.709 gamma curve, a histogram-based white level and the sRGB colorspace. The resizing algorithm used is the Bicubic kernel in Matlab.

A. The Correlations Between Channels

To study the correlations between color image channels, we will analyze the interaction between different channels in the process of color image formation.

For color images, when we need to collect a variety of basic colors, such as R, G and B colors, the easiest method is to use the filter method, i.e., the three wavelengths pass through three corresponding filters. The best choice for collecting the three basic colors of RGB is using the Bayer format, which was invented by Bayer [29]. The Bayer format uses twice as many green pixels as red or blue to mimic the physiology of the human eye. Fig. 1 shows the image capture process in a digital camera. The filtered light is sensed by the sensor and passed through an analog-to-digital converter. After that, it is stored in a raw image. However, each channel of the raw image has many empty pixels. Therefore, CFA interpolation is performed to make the raw image similar to the original scene. The Bayer image study shows that the green component contains the main luminance information, and it has strong spatial and spectral correlations with the red and blue components, thereby playing a key role in reconstructing high-quality full-color images. Therefore, the G channel contains more raw information, and most demosaicing algorithms give priority to the G channel.

To measure the strength of the correlations, we will use the Pearson correlation coefficient [30] to quantify the correlation between the two channels. We denote $Corrcoef(\mathbf{R}, \mathbf{G})$ as the Pearson correlation coefficient value of $\mathbf{R}$ and $\mathbf{G}$. A larger $Corrcoef$ indicates that the two channels are very similar or have a stronger correlation. We compute the Pearson correlation coefficient between two of the three channels of each image in BOSSbasePPGBIC and then compute the average of the $Corrcoef(\mathbf{R}, \mathbf{G})$, $Corrcoef(\mathbf{R}, \mathbf{B})$ and $Corrcoef(\mathbf{G}, \mathbf{B})$ values of these images to obtain $Corrcoef_{avg}(\mathbf{R}, \mathbf{G}) = 0.9399$, $Corrcoef_{avg}(\mathbf{R}, \mathbf{B}) = 0.8284$ and $Corrcoef_{avg}(\mathbf{G}, \mathbf{B}) = 0.9101$. Obviously, $Corrcoef_{avg}(\mathbf{R}, \mathbf{G})$ and $Corrcoef_{avg}(\mathbf{G}, \mathbf{B})$ are much stronger than $Corrcoef_{avg}(\mathbf{R}, \mathbf{B})$. In addition, we validate some non-Bayer format sample images from DEREVIEW (https://www.dpreview.com). The results are shown in TABLE I. The results seem to imply that this relationship exists in the non-Bayer format as well. Therefore, we should pay greater attention to the G channel in color image steganography.

B. The Strategy of Clustering Modification Directions Between Channels

In [9], the CMD was proposed to preserve the correlations between neighbouring pixels. Motivated by the excellent performance of the CMD, a strategy called CMD-C (clustering

TABLE I
THE CORRELATION BETWEEN NON-BAYER FORMAT COLOR IMAGE CHANNELS

Device	Color Filter Array	Number	$Corrcoef_{avg}(\mathbf{R},\mathbf{G})$	$Corrcoef_{avg}(\mathbf{R},\mathbf{B})$	$Corrcoef_{avg}(\mathbf{G},\mathbf{B})$
Fujifilm X-T30	X-Trans	49	0.9532	0.8898	0.9577
Huawei P30 Pro	RYYB	37	0.9630	0.9155	0.9468
Sony DSC-F828	RGBE	20	0.8093	0.7342	0.9050

TABLE II
DIFFERENT THREE-CHANNEL EMBEDDING PATTERNS AND THEIR STEGANALYSIS RESISTANCE

	Pattern A	Pattern B	Pattern C	Pattern D	Pattern E	Pattern F
Modes for **R**-**G**-**B**	$BASIC(\mathbf{R})$ $SYN(\mathbf{G},\mathbf{R})$ $SYN(\mathbf{B},\mathbf{R})$	$BASIC(\mathbf{G})$ $SYN(\mathbf{R},\mathbf{G})$ $SYN(\mathbf{B},\mathbf{G})$	$BASIC(\mathbf{B})$ $SYN(\mathbf{R},\mathbf{B})$ $SYN(\mathbf{G},\mathbf{B})$	$BASIC(\mathbf{R})$ $ASYN(\mathbf{G},\mathbf{R})$ $ASYN(\mathbf{B},\mathbf{R})$	$BASIC(\mathbf{R})$ $SYN(\mathbf{G},\mathbf{R})$ $ASYN(\mathbf{B},\mathbf{R})$	$BASIC(\mathbf{R})$ $ASYN(\mathbf{G},\mathbf{R})$ $SYN(\mathbf{B},\mathbf{R})$
CRMQ1	0.3051	0.3111	0.2991	0.2079	0.2067	0.1561
SCRMQ1	0.2555	0.2682	0.2548	0.2098	0.2069	0.1607

modification directions for color components) [23] was later proposed. That method aims to preserve not only correlations between neighbouring pixels but also the correlations among the three channels. However, the actual performance of CMD-C is not as expected because of the experimental setup. This is because the authors did not pay attention to the correlations between channels. In [23], Tang et al. performed a simulation to verify a useful idea, that the same modification direction at the same pixel location among the three color channels is effective in enhancing empirical security. This is a good conclusion, except for the simulation in that it only synchronizes the three color components of one pixel based on the **R**. However, we have previously analyzed that the **G** has a higher correlation than the **R** and **B**. Therefore, we will further expand and improve upon this simulation experiment to explore the impact of different embedding orders on the steganography security.

In this simulation, we use the BOSSbasePPGBIC as our database. HILL-CMD [9] is used as the baseline method, and the payload is set to 0.4 bpcp (bits per channel pixel). We will use six patterns to create six stego image sets. Taking pattern A in TABLE II as an example, messages are embedded into **R** using the HILL-CMD denoted as $BASIC(\mathbf{R})$, and the modification directions of the pixels in **R** are copied to the other two channels, denoted as $SYN(\mathbf{G},\mathbf{R})$ and $SYN(\mathbf{B},\mathbf{R})$. In contrast to SYN, $ASYN$ means that the modification directions are opposite. The two feature sets CRMQ1 and SCRMQ1 [13], which are powerful enough to detect the correlations among the channels, are used to evaluate the security. The ensemble classifier [31] is fed the extracted features. The anti-detection performance is evaluated by the testing error, which is the mean of the false alarm rate and the missed detection rate over 10 runs using 5000/5000 database splits. A larger testing error means stronger security.

The experimental results are shown in TABLE II. We can see that patterns A, B, and C belong to the same class; however, their performances are different. In these three patterns, the modification directions of the three channels are the same, except that the fundamental modifications are different. Among them, pattern B is the most secure, and its basic modifications are derived from **G**. Patterns D, E, and F belong to another class; they have the same fundamental modifications; however, only two channels have the same modification directions, while the other channel is opposite to the two channels. Among them, pattern F, where the modification directions of **G** are opposite to those of **R** and **B**, shows the worst performance. The results again verify that **G** is not only a unique channel but also plays a crucial role in color image steganography. The results also show that the SMD rule cannot be used equally between the three channels. Therefore, we extend the SMD rule to the Intra-channel-SMD rule and the Inter-channel-SMD rule for the color image. The Intra-channel-SMD rule is the same as the SMD rule in the grayscale image and is used in the color channels. The Inter-channel-SMD rule will be used to guide the modification directions between the color channels.

To further explore the impact of synchronization or asynchronization between two channels on the performance of statistical undetectability for steganography, we will use another six patterns to create six stego image sets. Within the patterns, only two channels are embedded. The embedding method, payload and evaluation method are the same as before. The experimental results are shown in TABLE III. From patterns G, H, I and J, we can see that when **R** or **B** is synchronized with **G**, the performance is much better than the corresponding asynchronization. However, from patterns K and L, we can see that there is minimal difference in performance between **R** and **B** after synchronization or asynchronization. Moreover, the capacity of each pixel will be reduced when attempting to synchronize modification directions, and thus, the change rate will be increased for a given payload, which may reduce the steganography security. Therefore, it is not necessary to synchronize the modification directions of **R** and **B**. We propose that the Inter-channel-SMD rule should be used preferentially when there is a strong correlation.

TABLE III

DIFFERENT TWO-CHANNEL EMBEDDING PATTERNS AND THEIR STEGANALYSIS RESISTANCE

	Pattern G	Pattern H	Pattern I	Pattern J	Pattern K	Pattern L
Modes for **R-G-B**	$BASIC(\mathbf{G})$ $SYN(\mathbf{R},\mathbf{G})$	$BASIC(\mathbf{G})$ $ASYN(\mathbf{R},\mathbf{G})$	$BASIC(\mathbf{G})$ $SYN(\mathbf{B},\mathbf{G})$	$BASIC(\mathbf{G})$ $ASYN(\mathbf{B},\mathbf{G})$	$BASIC(\mathbf{R})$ $SYN(\mathbf{B},\mathbf{R})$	$BASIC(\mathbf{R})$ $ASYN(\mathbf{B},\mathbf{R})$
CRMQ1	0.3038	0.2231	0.3066	0.2173	0.2634	0.2506
SCRMQ1	0.2835	0.2319	0.2908	0.2349	0.2734	0.2612

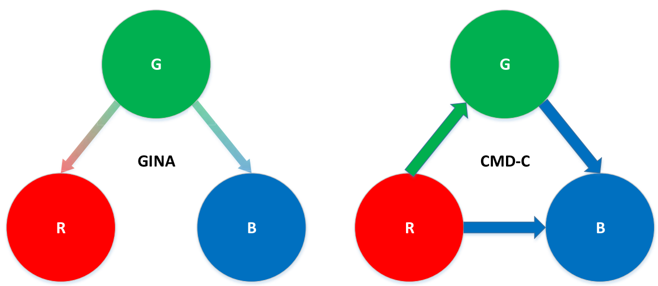

Fig. 2. The main difference between the GINA and CMD-C.

For color images, we should synchronize the modification directions of **R** and **B** according to **G**. The **G** should be embedded first, and then, **R** and **B** should be embedded according to **G**. Based on this idea, we design a new strategy for defining a non-additive cost for color image steganography, called G-channel-related Inter-channel Non-Additive (GINA). The GINA strategy will apply both the Intra-channel-SMD rule and the Inter-channel-SMD rule to the channels. The main difference between the GINA and CMD-C strategies is shown in Fig. 2, where **R** and **B** influence each other in the CMD-C but weakly influence each other in the GINA.

IV. THE DIFFERENCES BETWEEN CHANNELS

In the previous section, we found that **G** has a stronger correlation with **R** and **B** and proposed that the Inter-channel-SMD rule should be used preferentially when there is a stronger correlation between channels. However, it is not only the intensity of the correlation that varies between channels but also the payload capacity and the distribution of complex regions. In this section, we will first show the differences in the payload capacity and the distribution of complex regions between channels and then propose a new method to select the complex regions to apply the Inter-channel-SMD rule between channels.

A. The Capacity Differences Between Channels

In conventional steganographic schemes, we usually treat each color channel as a grayscale image independently for embedding and allocating the same payload. Because these schemes do not consider the differences among the three color channels, they may not minimize a distortion (detectability) over all pixels from the three channels. In [13], Goljan et al. confirmed that the red channel is the noisiest. Therefore, we should allocate more payload to the red channel.

TABLE IV

THE PERCENTAGE VALUE OF PAYLOAD PARTITION IN RGB CHANNELS UNDER DIFFERENT EMBEDDING PAYLOADS

Channel	0.1	0.2	0.3	0.4	0.5
R	52.46%	51.01%	49.76%	48.61%	47.51%
G	22.19%	22.32%	22.58%	22.93%	23.34%
B	25.35%	26.68%	27.66%	28.46%	29.15%

Because the SCC is simple and can distribute the payload adaptively, we will use it to explore the payload capacity between the three channels.

In this experiment, we randomly select 1000 color images from BOSSbasePPGBIC and then decompose each color image and merge the three channels into a single-channel image. We use HILL to compute the costs of the single-channel image and then obtain the average payload ratio of each channel over different total embedding payloads. The results are shown in TABLE IV. The payload partition using the SCC strategy is entirely different from the average payload assignment. Moreover, regardless of the payload, the average payload partition of **G** is the smallest. It seems that **G** is smoother than the other two channels. And We think that synchronizing with **G** to update the costs will lead to a lower rate of change. In this paper, we will use the SCC strategy to allocate the messages by default.

In the GINA strategy, we will apply the Inter-channel-SMD rule between two pairs of channels. However, the payload capacity between the channels is different. Therefore, we believe that the distributions of costs between channels are not similar and that the Inter-channel-SMD rule cannot be applied directly and indiscriminately between channels. In the next subsection, we will show the differences in the distributions of complex regions.

B. Distribution Differences of Complex Regions Between Channels

In Section III-A, we found that the **R** and **B** are similar to the **G**, but the distribution of complex regions may not be similar in some regions. Since the modification probability map can reflect the distribution of complex regions, here we provide an example to visualize the distribution between the three channels. A sample color image "5136.ppm", which is from the BOSSbasePPGBIC, as shown in Fig. 3(a). Fig. 3(b)-(d) are grayscale displays of the three channels. As we can see that the overall structure of each image is similar, but the

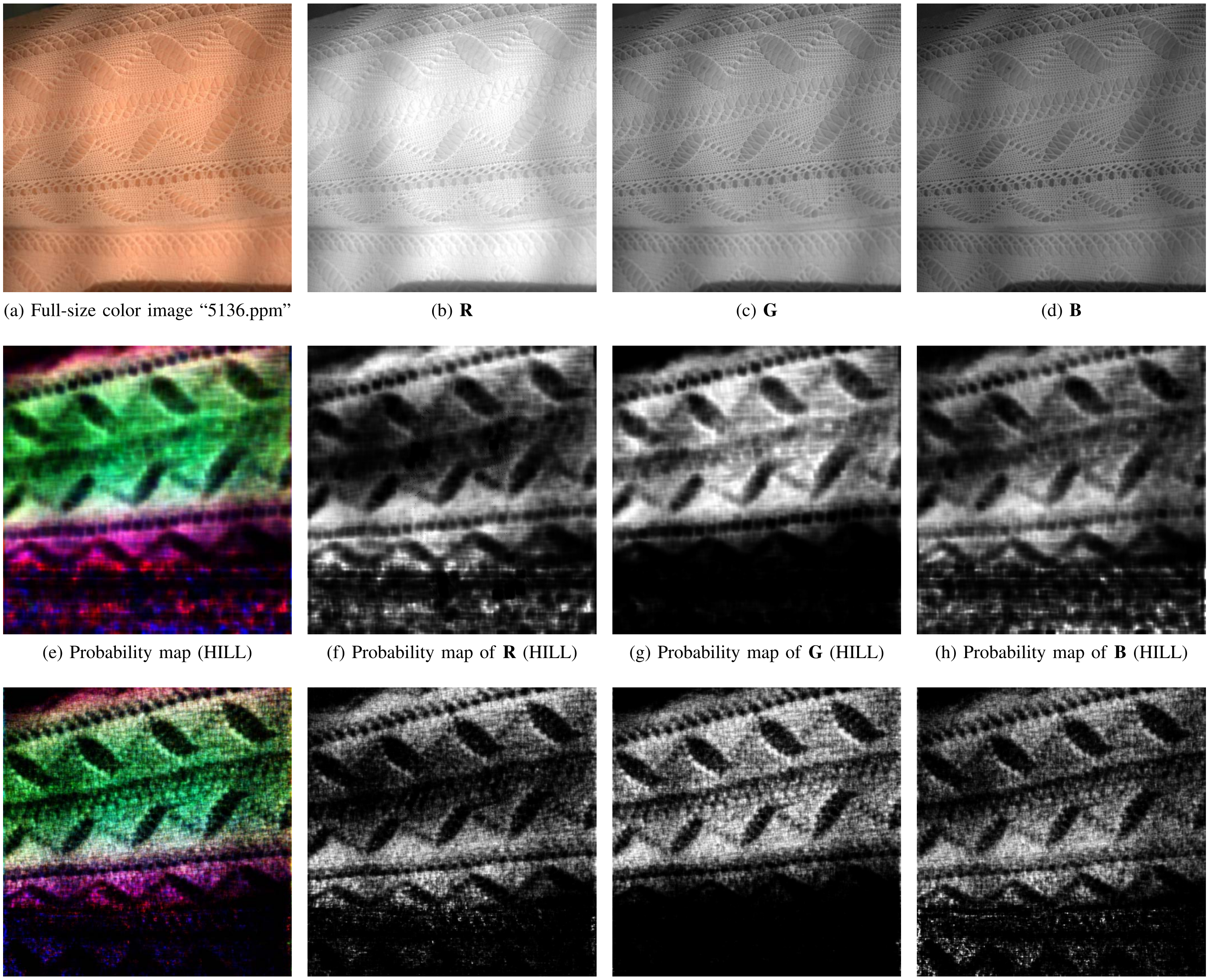

(a) Full-size color image “5136.ppm” (b) **R** (c) **G** (d) **B**

(e) Probability map (HILL) (f) Probability map of **R** (HILL) (g) Probability map of **G** (HILL) (h) Probability map of **B** (HILL)

(i) Probability map (WOW) (j) Probability map of **R** (WOW) (k) Probability map of **G** (WOW) (l) Probability map of **B** (WOW)

Fig. 3. The modification probability map for the three channels.

details are different. We use HILL and WOW applied with the SCC strategy to calculate the modification probability map with an embedding rate of 0.4 bpcp. For a more intuitive display, the probability is scaled and adjusted to $[0, 1]$. The higher the modification probability, the brighter the display. We show the modification probability map for the three channels in Fig. 3(e)-(l). We can see that the probability in the same position varies greatly in different channels. In this paper, we consider those high probability regions to be complex regions. Therefore, some regions are complex regions in the **G** but smooth regions in the **R** or **B**. If we update the costs of the **R** and **B** according to the modifications of the **G**, it will violate the Complexity Prior rule. As we know, the basic rule for cost assignment is the Complexity Prior rule, which gives the high priority for modification to the complex regions. Several effective cost functions in the spatial domain allocate pixel costs by measuring the complexity of the neighborhood. The high cost means low modification probability and vice versa. In fact, the CMD strategy also follows the Complexity Prior rule. Because those pixels modified in steganography are likely to be in textured regions and natural images are highly correlated in a local neighbourhood. Therefore, it is also reasonable to update the costs of surrounding pixels to make it easier to modify, and the Intra-channel-SMD rule does not conflict with the Complexity Prior rule. However, the distribution of complex regions between channels is not similar. When we adopt the Inter-channel-SMD rule directly between channels, once the cost is updated, the priority of the pixel for modification will be changed. However, this can break the order of priority of the pixels. And we believe that the Inter-channel-SMD rule should under the Complexity Prior rule between color channels. To solve this problem, we will select the complex regions to update the costs.

C. Selecting the Complex Regions to Apply Inter-Channel-SMD Rule

To avoid priority reversal when applying the Inter-channel-SMD rule, we will only update the costs of the complex regions. However, selecting the regions is a problem. In [32], Tang et al., from the position of the detector, proposed a strategy to narrow down the suspicious regions for steganalysis. The suspicious regions are the complex regions with lower embedding costs, which are located based on the t percent of pixels with the lowest costs. However, the threshold t makes the selected regions of each image the same size. In [22], Liao et al. proposed a probability threshold for determining the complex regions. However, the threshold is fixed and cannot be optimized.

In this paper, we will select the complex regions that can carry the top T percent of modified pixels with the highest modification probability. When we use the SCC strategy to allocate messages, we can obtain the modification probability map $\mathbf{\Pi^m} = \left(\pi^m_{i,j,k}\right)^{n_1 \times n_2 \times 3}$ of the cover image, and $\pi^m_{i,j,k}$ can be calculated by Formula (8). A high probability means high complexity, and the set of high-probability pixels $\boldsymbol{H}^T$ that can carry the top T percent of modified pixels with the highest modification probability have the following attributes:

$$\sum_{(i,j,k)\in \boldsymbol{H}^T} \pi^m_{i,j,k} = \left(\sum \pi^m_{i,j,k}\right) \times T\%, \tag{10}$$

$$\min_{(i,j,k)\in \boldsymbol{H}^T} \left|\pi^m_{i,j,k}\right| \geqslant \max_{(i,j,k)\notin \boldsymbol{H}^T} \left|\pi^m_{i,j,k}\right|. \tag{11}$$

Therefore, we only need to choose the optimal T. Once T is determined, the set of high-probability pixels $\boldsymbol{H}^T$ can be determined. The size of the set depends on not only on the threshold T, but also content adaptation and payload adaptation. It varies with the complexity of the image. In general, the larger T is, the larger the set. The best T to resist steganalysis can be determined experimentally, as in Section VI-C.

V. Employment of the GINA

In this section, we first present the framework of the GINA strategy. Then, we detail the embedding steps in the three channels.

A. Framework

It has been shown in Section III that when the modification directions are consistent with **G**, better resistance to detection will be obtained. According to this discovery, we generalized the CMD strategy for grayscale images to color images, and this generalized strategy is called GINA.

The processing flow of the GINA-based algorithm is shown in Fig. 4. We first decompose the color image into three grayscale channel images. Then, we embed the first segment of messages into **G** using the CMD-based algorithm. Next, we embed the last two segments of messages into **R** and **B** according to the modification directions of **G**. During the embedding processes in **R** and **B**, the costs of the pixels are selectively updated according to its neighbouring pixels in the same channel and the pixels in the same position in **G**. Finally, the three stego channel images are recombined into a color stego image.

For each channel image, adaptive steganographic schemes, such as WOW, S-UNIWARD and HILL, can be applied to

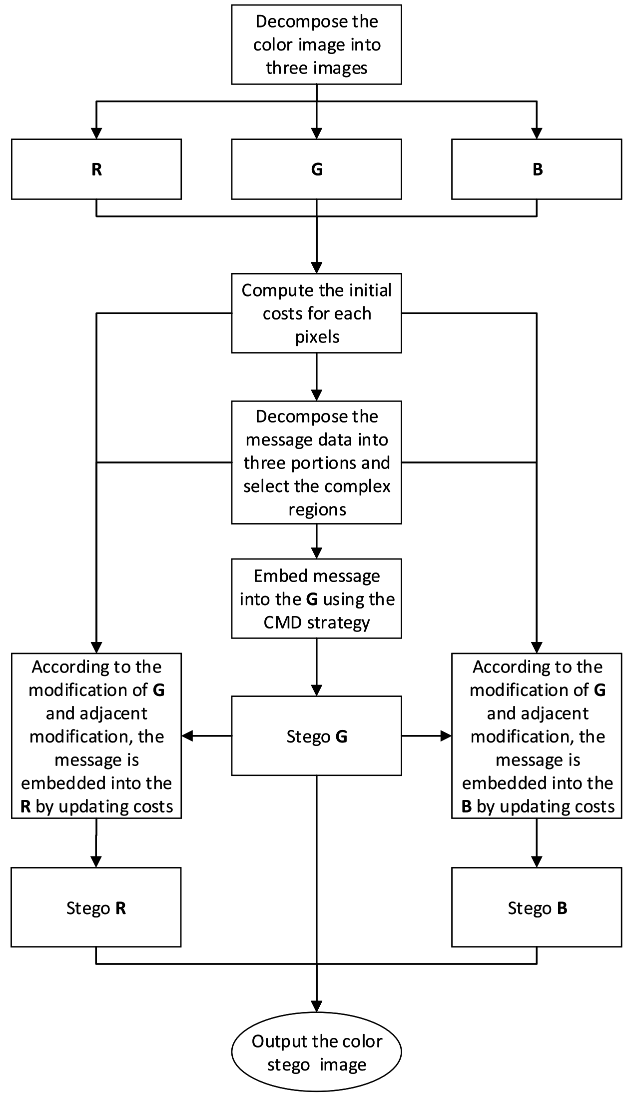

Fig. 4. Flowchart of the proposed solution used to incorporate the GINA strategy.

obtain the costs $\mathbf{C} = (c_{i,j,k})^{n_1 \times n_2 \times 3}$. At first, we set the initial costs $\rho^+_{i,j,k} = \rho^-_{i,j,k} = c_{i,j,k}$. The SCC strategy is used by default to make the messages of m bits adaptively distributed among the three channels. With the SCC strategy, we can get a modification probability map $\mathbf{\Pi^m} = \left(\pi^m_{i,j,k}\right)^{n_1 \times n_2 \times 3}$. We calculate the set of pixels $\boldsymbol{H}^T$ as the complex regions according to the threshold T, which will be determined experimentally in Section VI-C.

In the next two subsections, we will detail the embedding steps in the three channels.

B. Embedding in G Channel

According to the CMD strategy [9], we first decompose **G** into four disjoint sub-images. The set of pixels in the sub-image can be expressed as

$$S_{a,b,2} = \{x_{i,j,2} | i = a + 2k_a,\ j = b + 2k_b\}, \tag{12}$$

where $a \in \{1, 2\}$, $b \in \{1, 2\}$, $k_a \in \{0, 1, \cdots, \lfloor \frac{n_1}{2} \rfloor - 1\}$, $k_b \in \{0, 1, \cdots, \lfloor \frac{n_2}{2} \rfloor - 1\}$, and $\lfloor x \rfloor$ means rounding x down. As illustrated in Fig. 5(a), we embed the messages into the four

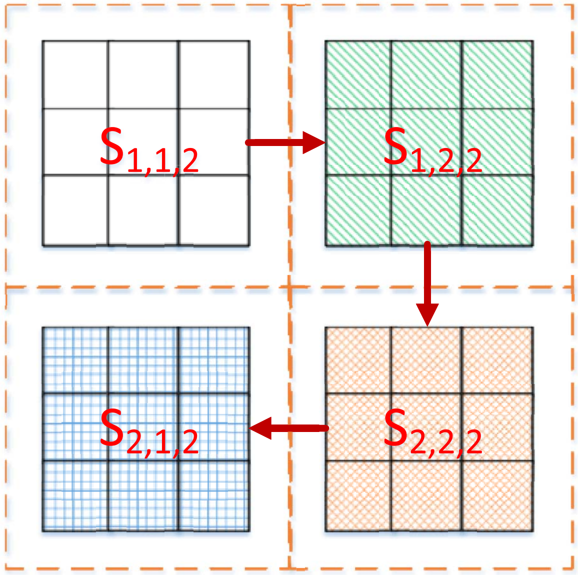

(a)

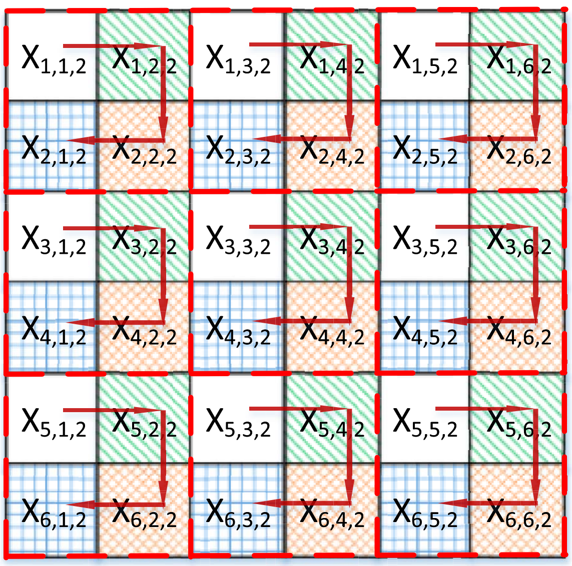

(b)

Fig. 5. Illustration of the embedding order. (a) An example embedding order for the four disjoint sub-images with horizontal zig-zag scan. (b) The embedding order in each red dotted sub-block of the sample G channel image.

sub-images in a horizontal zig-zag scan order, i.e., $S_{1,1,2} \rightarrow S_{1,2,2} \rightarrow S_{2,2,2} \rightarrow S_{2,1,2}$. Note that we embed messages into the pixels of each 2×2 sub-block in the same order, as shown in Fig. 5(b).

We intialize the stego image $\mathbf{Y} = \mathbf{X}$. For each sub-image, the length of the message to be embedded is equal. We first embed one quarter of messages into $S_{1,1,2}$ with the initial costs. After embedding the messages into $S_{1,1,2}$, we compute the difference between the stego image and the cover image $\mathbf{D} = \mathbf{Y} - \mathbf{X} = (d_{i,j,k})^{n_1 \times n_2 \times 3}$, and then, we update the costs of $S_{1,2,2}$ as follows:

$$\rho^{+}_{i,j,k} = \begin{cases} c_{i,j,k}/\alpha, & \text{if} \sum\limits_{(l,m,n)\in N_{i,j,k}} d_{l,m,n} > 0 \\ c_{i,j,k}, & \text{otherwise,} \end{cases} \tag{13}$$

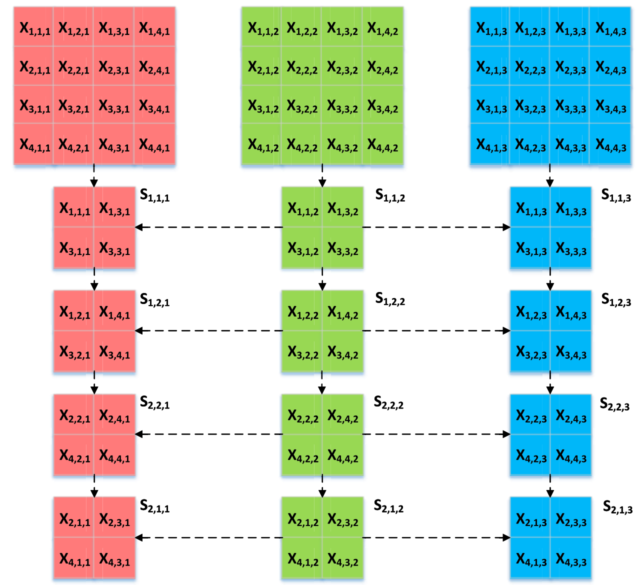

Fig. 6. An example embedding order for the 12 disjoint sub-images on the three channels.

and

$$\rho^{-}_{i,j,k} = \begin{cases} c_{i,j,k}/\alpha, & \text{if} \sum\limits_{(l,m,n)\in N_{i,j,k}} d_{l,m,n} < 0 \\ c_{i,j,k}, & \text{otherwise,} \end{cases} \tag{14}$$

where α is a scaling factor, and we set $\alpha = 9$ in this paper according to [9]. $N_{i,j,k}$ is the four-pixel neighbourhood of the pixel $x_{i,j,k}$ from the same channel, i.e., $x_{i-1,j,k}$, $x_{i+1,j,k}$, $x_{i,j-1,k}$, and $x_{i,j+1,k}$. When the pixel is on the image boundary, we use the available pixels in the four-pixel neighbourhood. After embedding the message into $S_{1,2,2}$ with the updated costs, we recalculate the difference $\mathbf{D}$ and then update the costs of $S_{2,2,2}$ as before. The same steps are used to embed the message into $S_{2,1,2}$ after we embed message into $S_{2,2,2}$. After we embed messages into the four sub-images, we can get a stego $\mathbf{G}$. In the next subsection, we will detail the embedding steps in the R and B channels.

C. Embedding in R and B Channels

After embedding the messages into the G channel, we embed the rest of messages into the R and B channels according to the modifications on the G channel. Similar to the decomposition in the $\mathbf{G}$, we first decompose the $\mathbf{R}$ and $\mathbf{B}$ into four sub-images respectively. The embedding order in $\mathbf{R}$ and $\mathbf{B}$ is the same as that in $\mathbf{G}$, as shown in Fig. 6.

On the same channel, we embed a message with the same length into each sub-image. Before embedding, we first compute the difference $\mathbf{D}$ and then update the costs of $S_{1,1,1}$ and $S_{1,1,3}$. The cost update will consider the modifications on $\mathbf{G}$ and the positions of the pixels. For the pixels in the complex regions, we update the costs considering the modification directions on $\mathbf{G}$. Therefore, the costs of $S_{1,1,1}$ and $S_{1,1,3}$ with

TABLE V
THE PERFORMANCE WITH DIFFERENT CHANNEL EMBEDDING ORDERS

Embedding Order	Features		Change Rate				Same Direction Rate		
	CRMQ1	SCRMQ1	**R**	**G**	**B**	Mean	SDR(**G**,**R**)	SDR(**G**,**B**)	SDR(**R**,**B**)
HILL-*RINA*	0.2843	0.2618	0.1515	0.0878	0.1080	0.1158	0.3669	0.3732	0.3374
HILL-*BINA*	0.3206	0.2816	0.1609	0.0852	0.0917	0.1126	0.2150	0.5391	0.2752
HILL-GINA	**0.3453**	**0.3078**	0.1586	0.0763	0.1002	0.1117	0.3128	0.5286	0.1785

$(i, j, k) \in \boldsymbol{H}^T$ are updated by

$$\rho^{+}_{i,j,k} = \begin{cases} c_{i,j,k}/\alpha, & \text{if } d_{i,j,2} > 0 \\ c_{i,j,k}, & \text{otherwise,} \end{cases} \tag{15}$$

and

$$\rho^{+}_{i,j,k} = \begin{cases} c_{i,j,k}/\alpha, & \text{if } d_{i,j,2} < 0 \\ c_{i,j,k}, & \text{otherwise,} \end{cases} \tag{16}$$

for $(i, j, k) \notin \boldsymbol{H}^T$, the costs of $S_{1,1,1}$ and $S_{1,1,3}$ will not be updated. After updating the costs of the pixels in the complex regions, we embed the corresponding message into $S_{1,1,1}$ and $S_{1,1,3}$ repectively. After this embedding, we recalculate the difference $\mathbf{D}$ and then update the costs of $S_{1,2,1}$ and $S_{1,2,3}$ considerring modifications to the neighbouring pixels and part of $\mathbf{G}$. For $(i, j, k) \in \boldsymbol{H}^T$, the costs of $S_{1,2,1}$ and $S_{1,2,3}$ are updated as follows:

$$\rho^{+}_{i,j,k} = \begin{cases} c_{i,j,k}/\alpha, & \text{if } \sum\limits_{(l,m,n)\in N_{i,j,k}} d_{l,m,n} + d_{i,j,2} > 0 \\ c_{i,j,k}, & \text{otherwise,} \end{cases} \tag{17}$$

and

$$\rho^{-}_{i,j,k} = \begin{cases} c_{i,j,k}/\alpha, & \text{if } \sum\limits_{(l,m,n)\in N_{i,j,k}} d_{l,m,n} + d_{i,j,2} < 0 \\ c_{i,j,k}, & \text{otherwise,} \end{cases} \tag{18}$$

for $(i, j, k) \notin \boldsymbol{H}^T$, we update the costs according to (13) and (14), the same as the updating on $\mathbf{G}$. After embedding messages into $S_{1,2,1}$ and $S_{1,2,3}$ with the updated costs, we recalculate the difference $\mathbf{D}$ and then update the costs of $S_{2,2,1}$ and $S_{2,2,3}$ as before. The same steps are used to embed the messages into $S_{2,1,1}$ and $S_{2,1,3}$ after we embed messages into $S_{2,2,1}$ and $S_{2,2,3}$. At last, we can get the three stego channel images and recombine them into a color stego image.

In this paper, we use S-UNIWARD and HILL to initialize the costs. And the corresponding schemes are called S-UNIWARD-GINA and HILL-GINA, respectively.

VI. Experimental Results and Analysis

A. Setups

In this section, all experiments except for the two described in subsections VI-F and VI-G are carried out on BOSSbasePPGBIC, which has been described in Section III. For the sake of simplicity, we use the optimal embedding simulator as the default and different seeds are used between the three channels in each round of embedding. Except for subsection VI-G, the performance is evaluated by the steganalyzer using the 18,157-dimensional SCRMQ1 and 5,404-dimensional CRMQ1 [13] feature sets with the ensemble classifier, and the performance quantification is the same as that described in Section III-B.

B. Impact of the Embedding Order

In Section III-B, we performed a simulation to confirm that it is better when the modification directions between channels are synchronized with $\mathbf{G}$ and worse when reversed. Here, we will compare the anti-detection performance of the GINA with the other two embedding orders when updating the costs. We call the other two embedding orders *RINA* and *BINA*. Taking *RINA* as an example, we replace $\mathbf{G}$ in GINA with $\mathbf{R}$ such that $\mathbf{R}$ is embedded first. The other two channels are embedded according to $\mathbf{R}$. The threshold T defaults to 100. The classification errors and the change rates are reported in TABLE V. We also calculate the same direction rate (SDR) of three pairs of channels. For example, SDR($\mathbf{G}$,$\mathbf{R}$) means the proportion of $\mathbf{G}$ and $\mathbf{R}$ having the same modifications in across all modified pixels. It can be observed that the GINA is the most secure embedding order in the natural color images. This again proves the importance of the $\mathbf{G}$. The mean change rate of the GINA is the lowest, and the sum of the values of SDR($\mathbf{G}$,$\mathbf{R}$) and SDR($\mathbf{G}$,$\mathbf{B}$) is higher than that of the other two embedding orders. In contrast, *RINA* has the worst performance. We believe that this is caused by two reasons. First, $\mathbf{R}$ has a lower Corrcoef value compared to the other two channels, as computed in Section III-A, and synchronizing with $\mathbf{R}$ is not the best choice. Second, $\mathbf{R}$ has a higher payload partition and change rate, as shown in TABLE IV and TABLE V; thus, more costs will be updated based on the modifications of $\mathbf{R}$, and the average rate of change will increase.

C. Impact of the Threshold

With the GINA strategy, a different threshold T will update different numbers of costs. We will use different thresholds from 0 to 100 to test the performance against CRMQ1 and SCRMQ1. When $T = 0$, the costs of $\mathbf{R}$ and $\mathbf{B}$ are not updated according to the modification of $\mathbf{G}$, whereas $T = 100$ is equivalent to updating all costs of $\mathbf{R}$ and $\mathbf{B}$ according to the modifications of $\mathbf{G}$. The result is shown in Fig. 7. We show the relation between the change rate and the threshold T in Fig. 8. The same direction rate is shown in Fig. 9. It can be observed that when the threshold increases, the performance against the CRMQ1 feature will be better because of the CRMQ1 formed by 3D co-occurrences across color channels. As shown in Fig. 9, with increased threshold T, more directions of modifications between channels will be in

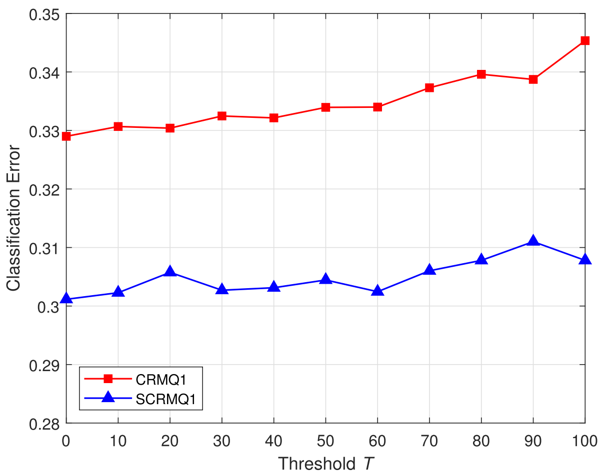

Fig. 7. Detection errors (CRMQ1 and SCRMQ1) for HILL-GINA with different threshold T.

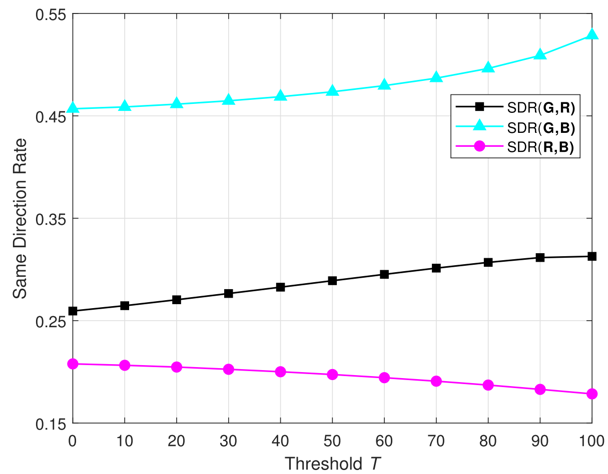

Fig. 9. The same direction rate with different threshold T.

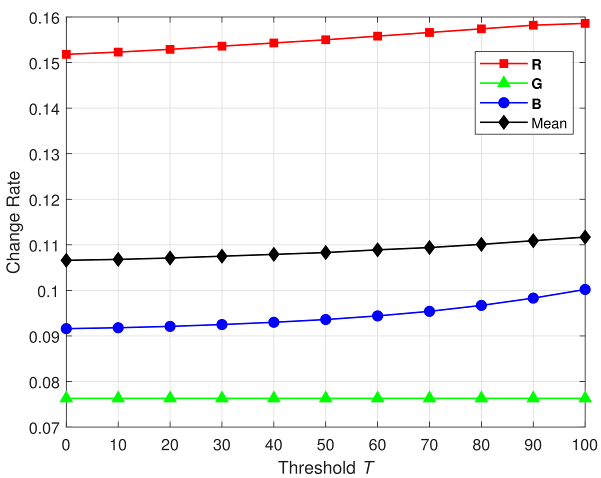

Fig. 8. Change rate for HILL-GINA with different threshold T.

the same direction, which is harder for CRMQ1 to detect. This also indicates that the GINA can indeed maintain the correlations between channels. However, the performance against SCRMQ1 first rises and then falls. This is because the distribution of the complex regions of **G** is not very similar to that of **R** and **B**, as discussed in Section IV-B. The larger the threshold is, the larger the area of the region in which the costs are selected to be updated, resulting in more costs of the non-textured regions being updated and the Complexity Prior rule being violated. It can be observed from Fig. 8 that the change rate grows as the threshold increases. Therefore, the trade-off between the Inter-channel-SMD rule and the Complexity Prior rule can be adjusted by the threshold T. Since the SCRMQ1 is the most effective steganalytic feature, we will refer to it to set the threshold $T = 90$ in the following experiments by default.

D. Impact of the Payload Partition

In this paper, we take the SCC strategy as a part of the GINA, and we use it to allocate the payload between the three channels. Moreover, there are two other payload partition strategies in the field of color image steganography. The traditional method is to treat the three channels equally as three grayscale images and allocate equal payloads. We call this the Average strategy. A new payload partition strategy called ACMP, which is based on amplifying channel modification probabilities, is an adaptive allocation strategy [22]. The authors stated that the ACMP strategy could allocate the payload by considering inter-channel correlations and can cluster the modifications in textured regions. The performance of HILL-GINA with the three payload partition strategies is shown in Fig. 10. It can be observed that for different payload rates and different steganalytic feature sets, the GINA with the SCC strategy could achieve better statistical undetectability. At low payload rates, the ACMP strategy is better than the Average strategy. However, when the embedding payload rate is higher, such as 0.4 and 0.5 bpcp, combining with the ACMP strategy will result in a worse performance than the Average strategy. We think the reason behind this is that the GINA combined with the ACMP will update the costs twice and disturb the distribution of the cost, resulting in more embedding changes. The average change rates for HILL-GINA with different payload partition strategies and different payloads are shown in Fig. 11. As the figure shows, the average change rates of the ACMP strategy increase beyond those of the SCC and Average strategy. Above all, the SCC strategy is selected in the GINA scheme.

E. Comparison to State-of-the-Art Methods

We compare the HILL-GINA and S-UNIWARD-GINA schemes with some currently popular methods, including HILL-CMD-C, S-UNIWARD-CMD-C using the CMD-C [23] strategy, HILL-CMD, S-UNIWARD-CMD, CPV-CMD using the CMD [9] strategy, HILL-ACMP, S-UNIWARD-ACMP using the ACMP [22] strategy and the initial cost HILL [7], S-UNIWARD [6] and CPV [24]. In this experiment, the payload ranges from 0.1 to 0.5 bpcp, and the CRMQ1 and SCRMQ1 feature sets are used to evaluate the performances. The results are shown in Fig. 12 and Fig. 13. We can observe

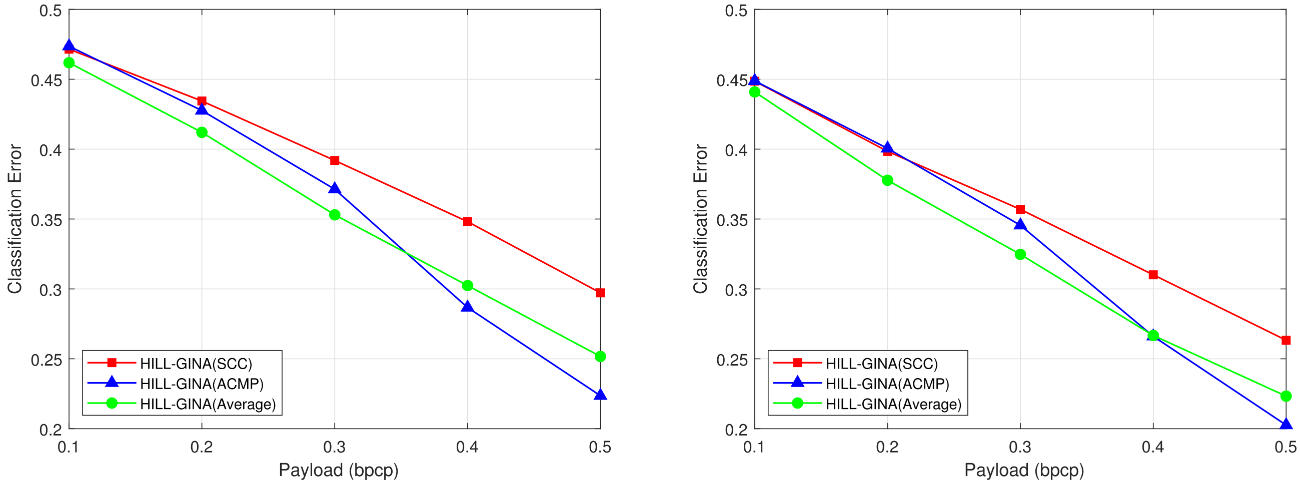

(a) (b)

Fig. 10. Detection errors for HILL-GINA with different payload partition strategies when steganalyzing with (a) CRMQ1 and (b) SCRMQ1.

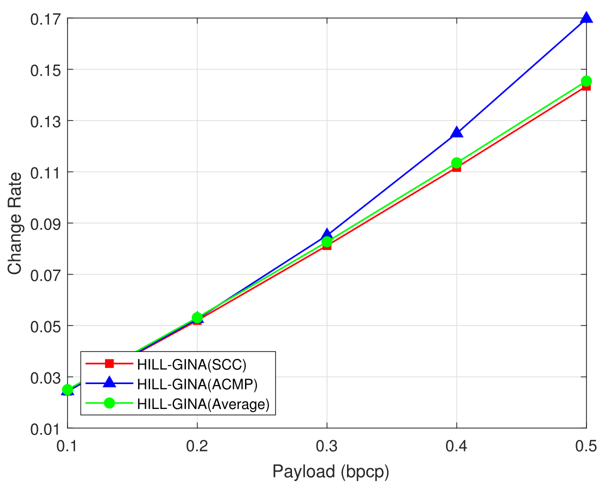

Fig. 11. Average rate of change for HILL-GINA with different payload partition strategies and different payloads.

that GINA-based schemes outperform the other steganographic schemes.

F. Performance on Other Datasets

To investigate whether the performance of the GINA is over-optimized on the BOSSbasePPGBIC database, we conduct several experiments on different color image databases. The image sets are obtained with the same steps as BOSSbasePPGBIC but with different demosaicking methods and post-processing operations. In this paper, four demosaicking methods (AHD, PPG, bilinear, and VNG) available in dcraw are used. Three common post-processing operations are considered: color transform, gamma correction and resize. The colorspace and gamma curve are set in dcraw, while the resize operation is set in Matlab. All images are resized or cropped to $512 \times 512 \times 3$. A total of 13 datasets are used to test the performance of the GINA.

The results are shown in TABLE VI. As we can see that the GINA outperforms other steganography methods in all of these scenarios. It can be concluded that the GINA can significantly improve the security on the other datasets, indicating that the GINA is not over-optimized on the BOSSbasePPGBIC (D6) database. In addition, we have some new findings as follows: 1). The demosaicking algorithm has minimal impact on the anti-detection performance when the colorspace, gamma curve and resize method are the same. 2). The color transform has a huge impact on the anti-detection performance. The steganographer can achieve better anti-detection performance for images generated with the Adobe RGB or sRGB colorspace. 3). Steganography in the gamma-corrected images will have a stronger anti-detection ability than in uncorrected images. 4). The anti-detection for steganography for the resized images is much higher than that for images that have simply been cropped, and the "Bicubic" method is better than the "Bilinear" method in color image steganography. Therefore, we recommend steganographers use resized color images in the sRGB or Adobe RGB colorspace and that are gamma corrected.

G. Performance on Resisting Other Steganalysis Methods

In addition to the SCRMQ1 and CRMQ1 features, there are other features and steganalysis methods. In [16], Abdulrahman et al. enriched the SCRMQ1 with an inter-channel correlation composed of three sets of features. The first set is SCRMQ1, and the other features are based on local Euclidean and mirror transformations, which can describe the consistency of the texture direction and reflect the correlations between channels. We call the two new features GTM, which are extracted from the co-occurrence correlation matrices formed by the sine and cosine of the gradient angles between all the color channels. Recently, deep convolutional neural networks have attracted increasing attention due to their excellent performance. In [33], Boroumand et al. proposed a deep residual network called SRNet, which

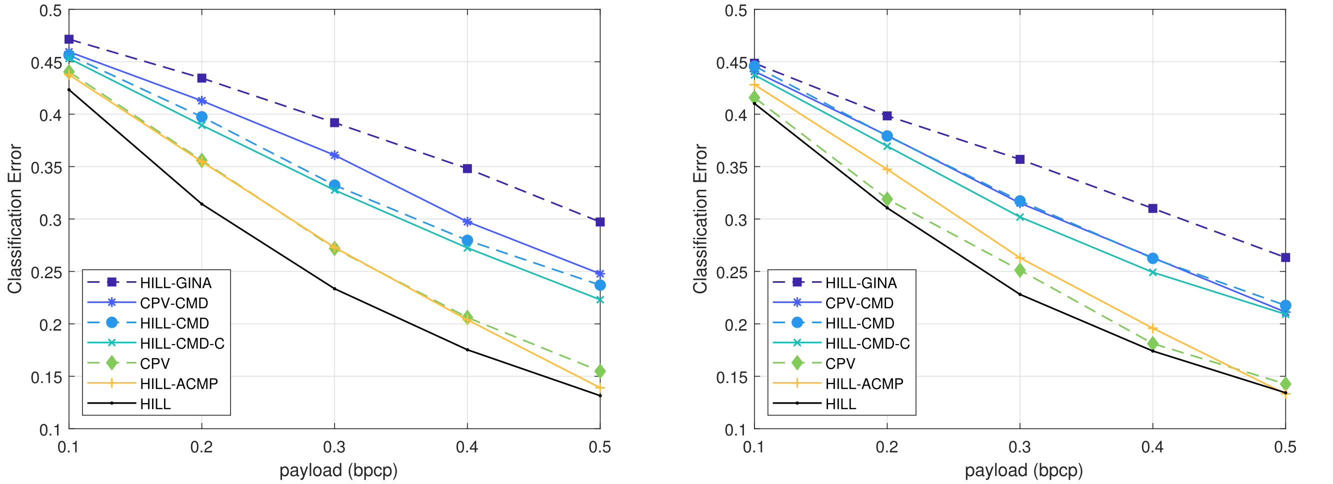

(a) (b)

Fig. 12. Comparison of HILL [7], CPV [24], ACMP [22], CMD [9], CMD-C [23] and GINA for resisting dection by (a) CRMQ1 and (b) SCRMQ1 [13] on BOSSbasePPGBIC.

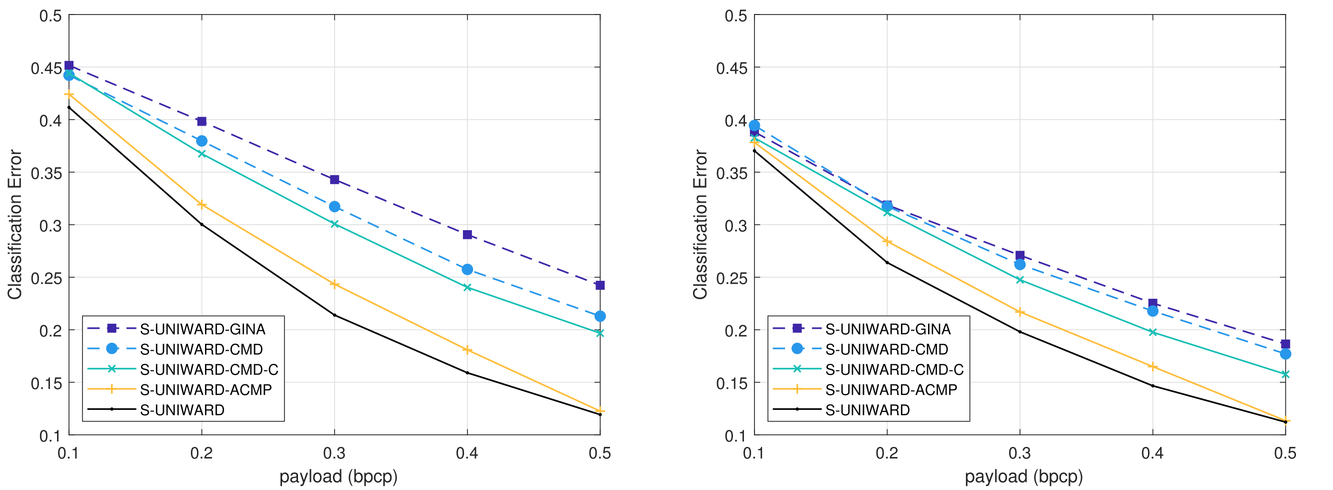

(a) (b)

Fig. 13. Comparison of S-UNIWARD [6], ACMP [22], CMD [9], CMD-C [23] and GINA for resisting dection by (a) CRMQ1 and (b) SCRMQ1 [13] on BOSSbasePPGBIC.

TABLE VI

DETECTION ERRORS ON DIFFERENT DATASETS FOR DIFFERENT STEGANOGRAPHIC SCHEMES UNDER 0.4 BPCP PAYLOAD

Datasets					CRM				SCRM			
Index	Demosaicking	Colorspace	Gamma curve	Resize	HILL	CMD-C	CMD	GINA	HILL	CMD-C	CMD	GINA
D1	PPG	RAW	BT.709	Bicubic	0.0591	0.1321	0.1330	**0.1831**	0.0612	0.1330	0.1382	**0.1838**
D2	AHD	RAW	BT.709	Bicubic	0.0603	0.1329	0.1326	**0.1814**	0.0625	0.1334	0.1368	**0.1787**
D3	Bilinear	RAW	BT.709	Bicubic	0.0721	0.1617	0.1586	**0.2094**	0.0753	0.1614	0.1622	**0.2045**
D4	VNG	RAW	BT.709	Bicubic	0.0565	0.1310	0.1299	**0.1759**	0.0603	0.1337	0.1399	**0.1718**
D5	PPG	Adobe RGB	BT.709	Bicubic	0.1513	0.2601	0.2664	**0.3032**	0.1543	0.2430	0.2521	**0.2791**
D6	PPG	sRGB	BT.709	Bicubic	0.1753	0.2725	0.2797	**0.3387**	0.1741	0.2492	0.2625	**0.3110**
D7	PPG	RAW	Linear	Bicubic	0.0421	0.0895	0.0910	**0.1322**	0.0431	0.0898	0.0949	**0.1280**
D8	PPG	sRGB	Linear	Bicubic	0.1050	0.1654	0.1816	**0.2327**	0.0999	0.1525	0.1683	**0.2087**
D9	PPG	RAW	BT.709	Bilinear	0.0167	0.0519	0.0576	**0.0931**	0.0184	0.0551	0.0622	**0.0948**
D10	PPG	RAW	BT.709	Only crop	0.0005	0.0005	0.0005	**0.0007**	0.0004	0.0004	0.0003	**0.0005**
D11	PPG	sRGB	BT.709	Only crop	0.0077	0.0067	0.0086	**0.0128**	0.0053	0.0048	0.0066	**0.0079**
D12	PPG	RAW	Linear	Only crop	0.0003	0.0006	0.0005	**0.0007**	0.0003	0.0003	0.0004	**0.0005**
D13	PPG	sRGB	Linear	Only crop	0.0028	0.0030	0.0031	**0.0032**	0.0026	0.0027	0.0027	**0.0030**

achieves state-of-the-art results in image steganalysis. In the ALASKA steganalysis challenge [34], Yousfi *et al.* [21] won the challenge using methods built around the same deep residual neural network SRNet.

To investigate whether the GINA-based method is effective in resisting steganalyzers equipped with enriched rich features or deep convolutional neural networks, we conducted additional experiments to test the anti-steganalysis performance.

TABLE VII

DETECTION ERRORS (SRNET AND SCRMQ1+GTM) ON BOSSBASEPPGBIC256 FOR DIFFERENT STEGANOGRAPHIC SCHEMES AND PAYLOADS

Steganalysis method	SRNet				(SCRMQ1+GTM)+Ensemble Classifier			
Payload (bpcp)	0.1	0.2	0.3	0.4	0.1	0.2	0.3	0.4
HILL	0.1756	0.1047	0.0681	0.0052	0.4181	0.3106	0.2184	0.1554
HILL-CMD-C	0.2366	0.1556	0.1092	0.0833	0.4519	0.3856	0.3146	0.2520
HILL-CMD	0.2287	0.1457	0.1095	0.0901	0.4564	0.3936	0.3245	0.2659
HILL-GINA	**0.2592**	**0.1889**	**0.1505**	**0.1205**	**0.4620**	**0.4140**	**0.3595**	**0.2980**

Due to the limited memory of our GPUs (10-11GB), in order to use a reasonable size minibatch, these network detectors were trained on small 256×256 tiles, and the cover images of BOSSbasePPGBIC were resized from $512 \times 512 \times 3$ to $256 \times 256 \times 3$ using *imresize* with the default settings in Matlab. We call this dataset BOSSbasePPGBIC256. The performance quantification of the enriched features is the same as that described in Section III-B. In SRNet, the image set is randomly split into a training set with 7,000 cover and stego image pairs and a validation set with 500 image pairs and the remaining images were used for testing. The training was first run for 442k iterations (480 epochs) with an initial learning rate of $r_1 = 0.001$ and then for an additional 100k iterations (109 epochs) with a learning rate of $r_2 = 0.0001$. We compare the detection performance of HILL, HILL-CMD, HILL-CMD-C and HILL-GINA with embedding payload rates of 0.1 to 0.4 bpcp. The results are shown in TABLE VII. It can be observed that the GINA-based method can also achieve better performance when detected by SRNet or SCRMQ1+GTM with Ensemble Classifier. Furthermore, the steganalysis based on the deep residual network has a better detection ability than the traditional machine learning method.

VII. CONCLUSION

With color images becoming the main medium for information communication, the corresponding requirements for powerful color image steganography have become increasingly urgent. In this paper, we proposed a novel strategy called the GINA for color image steganography considering the correlations and differences between the three channels. The strategy can be easily combined with state-of-the-art steganographic methods to improve steganographic security. The GINA strategy has two benefits. First, it can effectively cluster modification directions to maintain the correlations between channels and within the channel. Second, the GINA strategy can allocate the payload adaptively and has a lower change rate.

However, the GINA strategy is designed for color images in the RGB format. How to design non-additive cost functions for other color image formats, such as YCbCr [35], [36], is still an interesting problem. We will extend GINA to YCbCr format in the future work.

ACKNOWLEDGMENT

The authors would like to thank DDE Laboratory of SUNY Binghamton for sharing the source code of their steganography, steganalysis and ensemble classifier on the webpage (http://dde.binghamton.edu/download/).

REFERENCES

[1] T. Pevný and J. Fridrich, "Benchmarking for steganography," in *Proc. Int. Workshop Inf. Hiding*. Berlin, Germany: Springer, 2008, pp. 251–267, doi: 10.1007/978-3-540-88961-8_18.

[2] J. Fridrich, *Steganography in Digital Media: Principles, Algorithms, and Applications*. Cambridge, U.K.: Cambridge Univ. Press, 2009.

[3] T. Filler, J. Judas, and J. Fridrich, "Minimizing additive distortion in steganography using syndrome-trellis codes," *IEEE Trans. Inf. Forensics Security*, vol. 6, no. 3, pp. 920–935, Sep. 2011.

[4] T. Pevný, T. Filler, and P. Bas, "Using high-dimensional image models to perform highly undetectable steganography," in *Proc. Int. Workshop Inf. Hiding*. Springer, 2010, pp. 161–177.

[5] V. Holub and J. Fridrich, "Designing steganographic distortion using directional filters," in *Proc. IEEE Int. Workshop Inf. Forensics Secur. (WIFS)*, Dec. 2012, pp. 234–239.

[6] V. Holub, J. Fridrich, and T. Denemark, "Universal distortion function for steganography in an arbitrary domain," *EURASIP J. Inf. Secur.*, vol. 2014, no. 1, p. 1, 2014.

[7] B. Li, M. Wang, J. Huang, and X. Li, "A new cost function for spatial image steganography," in *Proc. IEEE Int. Conf. Image Process. (ICIP)*, Oct. 2014, pp. 4206–4210.

[8] V. Sedighi, R. Cogranne, and J. Fridrich, "Content-adaptive steganography by minimizing statistical detectability," *IEEE Trans. Inf. Forensics Security*, vol. 11, no. 2, pp. 221–234, Feb. 2016.

[9] B. Li, M. Wang, X. Li, S. Tan, and J. Huang, "A strategy of clustering modification directions in spatial image steganography," *IEEE Trans. Inf. Forensics Security*, vol. 10, no. 9, pp. 1905–1917, Sep. 2015.

[10] T. Denemark and J. Fridrich, "Improving steganographic security by synchronizing the selection channel," in *Proc. 3rd ACM Workshop Inf. Hiding Multimedia Secur.*, Jun. 2015, pp. 5–14.

[11] A. D. Ker *et al.*, "Moving steganography and steganalysis from the laboratory into the real world," in *Proc. 1st ACM Workshop Inf. Hiding Multimedia Secur.*, Jun. 2013, pp. 45–58.

[12] W. Zhang, Z. Zhang, L. Zhang, H. Li, and N. Yu, "Decomposing joint distortion for adaptive steganography," *IEEE Trans. Circuits Syst. Video Technol.*, vol. 27, no. 10, pp. 2274–2280, Oct. 2017.

[13] M. Goljan, J. Fridrich, and R. Cogranne, "Rich model for steganalysis of color images," in *Proc. IEEE Int. Workshop Inf. Forensics Secur. (WIFS)*, Dec. 2014, pp. 185–190.

[14] M. Goljan and J. Fridrich, "CFA-aware features for steganalysis of color images," in *Proc. SPIE, Media Watermarking, Secur., Forensics, Int. Soc. Opt. Photon.*, vol. 9409. Bellingham, WA, USA: SPIE, 2015, pp. 279–291.

[15] H. Abdulrahman, M. Chaumont, P. Montesinos, and B. Magnier, "Color image stegananalysis using correlations between RGB channels," in *Proc. 10th Int. Conf. Availability, Rel. Secur.*, Aug. 2015, pp. 448–454.

[16] H. Abdulrahman, M. Chaumont, P. Montesinos, and B. Magnier, "Color images steganalysis using RGB channel geometric transformation measures," *Secur. Commun. Netw.*, vol. 9, no. 15, pp. 2945–2956, 2016.

[17] H. Abdulrahman, M. Chaumont, P. Montesinos, and B. Magnier, "Color image steganalysis based on steerable Gaussian filters bank," in *Proc. 4th ACM Workshop Inf. Hiding Multimedia Secur.*, Jun. 2016, pp. 109–114.

[18] Y. Kang, F. Liu, C. Yang, L. Xiang, X. Luo, and P. Wang, "Color image steganalysis based on channel gradient correlation," *Int. J. Distrib. Sensor Netw.*, vol. 15, no. 5, 2019, Art. no. 1550147719852031.

[19] Y. Kang, F. Liu, C. Yang, X. Luo, and T. Zhang, "Color image steganalysis based on residuals of channel differences," *Comput. Mater. Continua*, vol. 59, no. 1, pp. 315–329, 2019.

[20] J. Zeng, S. Tan, G. Liu, B. Li, and J. Huang, "WISERNet: Wider separate-then-reunion network for steganalysis of color images," *IEEE Trans. Inf. Forensics Security*, vol. 14, no. 10, pp. 2735–2748, Oct. 2019.

[21] Y. Yousfi, J. Butora, J. Fridrich, and Q. Giboulot, "Breaking ALASKA: Color separation for steganalysis in JPEG domain," in *Proc. ACM Workshop Inf. Hiding Multimedia Secur.*, Jul. 2019, pp. 138–149.

[22] X. Liao, Y. Yu, B. Li, Z. Li, and Z. Qin, "A new payload partition strategy in color image steganography," *IEEE Trans. Circuits Syst. Video Technol.*, to be published.

[23] W. Tang, B. Li, W. Luo, and J. Huang, "Clustering steganographic modification directions for color components," *IEEE Signal Process. Lett.*, vol. 23, no. 2, pp. 197–201, Feb. 2016.

[24] X. Qin, B. Li, S. Tan, and J. Zeng, "A novel steganography for spatial color images based on pixel vector cost," *IEEE Access*, vol. 7, pp. 8834–8846, 2019.

[25] B. Li, S. Tan, M. Wang, and J. Huang, "Investigation on cost assignment in spatial image steganography," *IEEE Trans. Inf. Forensics Security*, vol. 9, no. 8, pp. 1264–1277, Aug. 2014.

[26] K. Chen, H. Zhou, W. Zhou, W. Zhang, and N. Yu, "Defining cost functions for adaptive jpeg steganography at the microscale," *IEEE Trans. Inf. Forensics Security*, vol. 14, no. 4, pp. 1052–1066, Apr. 2019.

[27] W. Zhou, W. Zhang, and N. Yu, "A new rule for cost reassignment in adaptive steganography," *IEEE Trans. Inf. Forensics Security*, vol. 12, no. 11, pp. 2654–2667, Nov. 2017.

[28] P. Bas, T. Filler, and T. Pevný, "'Break our steganographic system': The ins and outs of organizing BOSS," in *Information Hiding*. Berlin, Germany: Springer, 2011, pp. 59–70.

[29] B. E. Bayer, "Color imaging array," U.S. Patent 3 971 065 A, Jul. 20, 1976.

[30] K. Pearson, "VII. Mathematical contributions to the theory of evolution.—III. Regression, heredity, and panmixia," *Philos. Trans. Roy. Soc. London. A, Containing Papers Math. Phys. character*, vol. 187, pp. 253–318, Dec. 1896.

[31] J. Kodovský, J. Fridrich, and V. Holub, "Ensemble classifiers for steganalysis of digital media," *IEEE Trans. Inf. Forensics Security*, vol. 7, no. 2, pp. 432–444, Apr. 2012.

[32] W. Tang, H. Li, W. Luo, and J. Huang, "Adaptive steganalysis against WOW embedding algorithm," in *Proc. 2nd ACM Workshop Inf. Hiding Multimedia Secur.*, Jun. 2014, pp. 91–96.

[33] M. Boroumand, M. Chen, and J. Fridrich, "Deep residual network for steganalysis of digital images," *IEEE Trans. Inf. Forensics Security*, vol. 14, no. 5, pp. 1181–1193, May 2018.

[34] R. Cogranne, Q. Giboulot, and P. Bas, "The ALASKA steganalysis challenge: A first step towards steganalysis 'into the wild,'" in *Proc. ACM Workshop Inf. Hiding Multimedia Secur.*, New York, NY, USA, 2019, pp. 125–137.

[35] S. Hemalatha, U. D. Acharya, and A. Renuka, "Comparison of secure and high capacity color image steganography techniques in RGB and YCbCr domains," Jul. 2013, *arXiv:1307.3026*. [Online]. Available: https://arxiv.org/abs/1307.3026

[36] T. Taburet, L. Filstroff, P. Bas, and W. Sawaya, "An empirical study of steganography and steganalysis of color images in the JPEG Domain," in *Proc. Int. Workshop Digit. Watermarking*, Oct. 2018, pp. 290–303. [Online]. Available: https://hal.archives-ouvertes.fr/hal-01904482

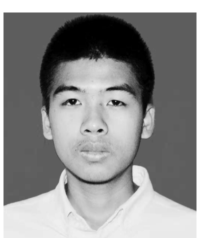

Yaofei Wang received the B.S. degree from the School of Physical Science and Technology, Southwest Jiaotong University, in 2017. He is currently pursuing the Ph.D. degree in information security with the University of Science and Technology of China. His research interests include information hiding, image processing, and deep learning.

Weiming Zhang received the M.S. and Ph.D. degrees from the Zhengzhou Information Science and Technology Institute, Zhengzhou, China, in 2002 and 2005, respectively. He is currently a Professor with the School of Information Science and Technology, University of Science and Technology of China. His research interests include multimedia security, information hiding, and privacy protection.

Weixiang Li received the B.S. degree from Xidian University, Xi'an, China, in 2016. He is currently pursuing the Ph.D. degree with the University of Science and Technology of China. His research interests include steganography and steganalysis. He was a recipient of the Best Student Paper Award of 6th ACM IH&MMSec in 2018.

Xinzhi Yu received the B.S. degree from the School of Electronics and Communication Engineering, Dalian University of Technology, in 2017. He is currently pursuing the M.S. degree in information security with the University of Science and Technology of China. His research interests include information hiding, image processing, and deep learning.

Nenghai Yu received the B.S. degree from the Nanjing University of Posts and Telecommunications in 1987, the M.E. degree from Tsinghua University in 1992, and the Ph.D. degree from the University of Science and Technology of China in 2004. He is currently a Professor with the University of Science and Technology of China. His research interests include multimedia security, multimedia information retrieval, video processing, information hiding and security, and privacy and reliability in cloud computing.